PHYSICAL REVIEW B VOLUME 3, NUMBER 5 1 MARCH 1971

Monte Carlo Channeling Calculations*

John H. Barrett
Solid State Division, Oak Ridge National Laboratory, Oak Ridge, Tennessee 37830
(Received 12 August 1970)

A Monte Carlo computer program for following the trajectories of high-energy ions in a lattice has been used to study depth dependence, half-angles, and minimum yields in channeling. The program uses the Thomas-Fermi interaction between ions and lattice atoms and gives the atoms' independent thermal displacements appropriate to the temperature of the lattice. The depth dependence of the nuclear interaction probability near the surface has been calculated and shown to be of importance in understanding other phenomena as well as having an intrinsic interest. Extensive calculations to explore the temperature and energy dependences of half-angles and minimum yields were done, and analytical formulas are given that summarize the computer results. The half-angle formulas give generally improved agreement with experiment and resolve certain discrepancies noted by Picraux, Davies, Eriksson, Johansson, and Mayer between their measurements and earlier theories. Minimum yields were calculated for both single- and double-alignment configurations. The results reveal an energy dependence as well as giving a better description of the temperature dependence and improved agreement with experiment. A relationship is given between the minimum yield and the yield from the surface.

I. INTRODUCTION

During the past several years much research has been devoted to the understanding and application of channeling and blocking. This work has been summarized in several reviews[1-3] and conference proceedings.[4-6] Two frequently measured aspects of these phenomena have been critical angles and minimum yields. Experimental results[7] have generally agreed rather well with predictions made by Lindhard[8] for critical angles but rather poorly with his predictions for minimum yields. Recently, Picraux *et al.*[9] have observed for materials of diamond structure deviations from Lindhard's results for critical angles even after including modifications to his results given by Andersen[10] for the effects of thermal vibrations. Part of these deviations has been accounted for by an extension of Lindhard's treatment made by Picraux and Andersen.[11] The theory developed in the present paper on critical angles is able to account for the results of Picraux *et al.* as well as other reported results. Minimum-yield results are also presented here for double as well as single-alignment configurations; they give an improved description of the temperature dependence and the first presentation of what energy dependence should be expected.

In the attempt to interpret the increasing number of experimental results that are available, it is necessary to analyze the implications of models of channeling in more detail and to consider more elaborate models. As the complexity of a set of calculations increases, the difficulties of analytical methods tend to rise more sharply than those of numerical methods. In addition, the repetitive nature of collisions in a solid and the random nature of thermal displacements are features of a calculation that can be handled very conveniently by a high-speed computer. Accordingly, an extensive series of Monte Carlo calculations has been undertaken, and the results, to be given below, illustrate the power of such techniques in the theory of channeling.

The first results presented are some on depth dependence, since the other calculations are influenced by them. Then the main results of the paper, based on Monte Carlo calculations of the temperature and energy dependences of axial and planar critical angles and minimum yields, are presented. Several formulas are also given which have been fitted to the Monte Carlo results and extend their usefulness by making analytical expressions available.

II. DESCRIPTION OF MONTE CARLO CALCULATIONS

Most of the results given below have been produced by a computer program for following trajectories of ions through a lattice. The main features of this program are as follows:

(i) Calculations may be done for elemental materials that have the body-centered cubic, face-centered cubic, and diamond structures. The program is written to give maximum efficiency for directions near the most open axial direction in a lattice. From the many possible combinations of beam and target materials and beam energies, certain ones were selected for extensive calculations because they were early or frequent experimental subjects or because of some interesting feature.

(ii) The motion of the ions is treated classically. Such a treatment was examined by Lindhard[12] and found to be valid for protons and heavier particles.

(iii) For channeling calculations, the starting points of trajectories are generally selected at random over the surface of the crystal by means of

a random-number generator but may be selected in other ways for special purposes. Random numbers may also be used to simulate the divergence of the beam and the mosaic spread of the target; Gaussian distributions have been used for these purposes, but other forms could easily be substituted if desired. The treatment of mosaic spread is applicable to thin-film crystals having large enough mosaic blocks that most ions pass through the crystal within the same mosaic block they enter at the incident surface.

(iv) For blocking calculations, the trajectories start from the position of a lattice atom, either at rest or at a position determined by thermal vibration. It would also be possible to start them from an interstitial site if desired. To determine the intensity of emergent particles in a given direction, it is necessary to start a large number of trajectories over a rather large solid angle surrounding that direction. This makes the program inefficient for most blocking calculations.

(v) Thermal vibrations may be simulated by giving each lattice atom a random displacement with the coordinates x, y, and z chosen from Gaussian distributions having the form

$$P(x) = (2\pi u_1^2)^{-1/2} \exp(-\tfrac{1}{2} x^2/u_1^2) , \quad (1)$$

where

$$u_1 = \langle x^2 \rangle^{1/2} = \langle y^2 \rangle^{1/2} = \langle z^2 \rangle^{1/2} .$$

The value of u_1 is computed from the Debye theory of thermal vibrations.[13] Values of the Debye temperature used in the calculations to be described below were 170 °K for gold,[14] 400 °K for tungsten,[15] 428 °K for aluminum,[15] 543 °K for silicon,[16] 290 °K for germanium,[16] and 2000 °C for diamond.[17] In order to economize on computer time, displacements with the above distributions are selected by a table look-up procedure in which the entry taken from the table is chosen by a random-number generator. Alternatively, calculations can be done for a static lattice.

(vi) Any desired form may be used for the interaction energy of the moving ion and a lattice atom. The one used for the calculations of the present paper was Molière's[18] approximation to the Thomas-Fermi function

$$V(r) = (Z_1 Z_2 e^2/r) \textstyle\sum_i \alpha_i e^{-\beta_i r/a} , \quad (2)$$

where $Z_1 e$ is the charge of the incident nucleus, $Z_2 e$ is the charge of the target nucleus, a is the screening length, i ranges from 1 to 3, $\{\alpha_i\} = \{0.1, 0.55, 0.35\}$, and $\{\beta_i\} = \{6.0, 1.2, 0.3\}$. The screening length used for ions that could be expected to be completely ionized was the Thomas-Fermi value for the target atom only,

$$a = 0.885 a_0 Z_2^{-1/3} , \quad (3a)$$

where a_0 is the Bohr radius. The value used for ions that were only partially ionized was one suggested by Firsov,[19]

$$a = 0.885 a_0 (Z_1^{1/2} + Z_2^{1/2})^{-2/3} . \quad (3b)$$

Firsov set down Eq. (3b) to apply to interactions between neutral atoms. Applying it, as done here, to an ion-atom interaction may be expected to give a value for the screening length that is somewhat small. However, (3b) should be better than (3a) for low degrees of ionization.

(vii) It is assumed that the ion has only one important interaction at a time as it moves through the lattice. The deflection at each interaction is computed by the impulse approximation. Following the methods given by Lehmann and Leibfried,[20] one may conclude that this approximation is valid if the energy E of the ion satisfies

$$E \gtrsim Z_1 Z_2 \times 300 \text{ eV} . \quad (4)$$

Appreciable amounts of computer time are saved by calculating a table of deflection as a function of impact parameter from the impulse approximation and looking up the value for each collision.

(viii) Energy losses by the ions are neglected. This omission is generally expected to have little effect unless one is looking specifically at energy losses or unless the ions lose a large fraction of their incident energy during passage through the crystal. In many of the calculations the ion energy used was the average value along the path rather than the incident value.

(ix) It is possible to compute a number of output quantities of interest. The most useful of these is the probability that an ion may have a sufficiently close nuclear encounter to cause an event such as a nuclear reaction, a large angle scattering of the ion, or a high-energy recoil of a lattice atom. These processes can be put on an equal footing if each is expressed as a normalized nuclear encounter probability, defined as the ratio of the cumulative probability computed in the course of a series of trajectories to the cumulative probability for an equal number of randomly oriented trajectories through an equal distance within the lattice. The motion of an ion past many different lattice sites is equivalent to the motion of many ions past a single site, each passage making a δ-function contribution to the flux of particles. The nuclear encounter probability is the cross section for the process times the integral of the product of the ion flux and the probability of a lattice atom being at the point of passage. For a frame of reference a major row direction near the beam direction is used. Let x and y be the coordinates perpendicular to this row, d the spacing along the row, and ψ the angle of the beam direction from the row. The area in the x-y plane associated with the row is $(Nd)^{-1}$, where N is

the density of atoms in the lattice. The normalized nuclear encounter probability is

$$P = \frac{\cos\psi}{2\pi u_1^2 N d \mathfrak{N}_c} \sum_{i=1}^{\mathfrak{N}_c} \exp\left(-\frac{x_i^2+y_i^2}{2u_1^2}\right), \quad (5)$$

where i labels the individual collisions and $\mathfrak{N}_c$ is the "number of collisions." $\mathfrak{N}_c$ is given by the number of trajectories multiplied by the thickness of the crystal divided by d. Other output quantities that can be readily obtained are the normalized number of lattice atoms having recoil energies greater than a specified amount and the angular distribution of the emergent beam.

(x) Estimates are made of the uncertainties in calculated values which arise because of the finite number of trajectories computed. This is done by dividing each group of trajectories for a given set of conditions into several batches, computing separate results for each batch, finding the mean value for the whole group, and computing the standard deviation of the batch values from the mean. These standard deviations will generally be presented along with the Monte Carlo results as error bars or error limits to indicate the uncertainties of calculation. Unless stated otherwise, the absence of error bars on a graph indicates that they are smaller than the symbol used in plotting the points.

(xi) The program is designed to run on either of the IBM system/360 computers that are available locally, a model 75 and a model 91. Part of the program is written in IBM FORTRAN IV and part in a local FORTRAN dialect. About 2000 collisions per second can be computed on the model 75 and 6000 on the model 91.

III. DEPTH DEPENDENCE

When an ion beam is directed along a channeling direction of a crystal, the nuclear encounter probability will vary with depth. This variation has two ranges, near the surface and deep in the bulk of the crystal, that show quite different behavior.

A. Surface Region

The depth dependence in the vicinity of the surface can be understood more readily than the dependence in the bulk of the crystal. Also, the behavior for a planar channel is easier to understand than that for an axial channel since the motion transverse to the channel direction is basically one dimensional in the planar case and two dimensional in the axial case. Figure 1 shows an example of the depth dependence in the region at and near the surface for a beam of 0.4-MeV protons incident parallel to the $(1\bar{1}1)$ channel in aluminum. Because the ions strike the surface of the crystal at random, the normalized nuclear encounter probability at zero depth is 1. As the beam proceeds into the crystal, the ions are repelled away from the walls of the channel, and there is a minimum at some small depth into the crystal. The trajectories that entered the crystal near a channel wall move through the center of the channel and across to the opposite wall, causing a peak at a somewhat greater depth in the crystal. These trajectories continue to oscillate back and forth across the channel and produce a series of maxima and minima at various depths in the crystal. Because such large amplitude trajectories all have about the same wavelength in the channel, the maxima and minima have a regular spacing. The half-wavelength for trajectories that enter the channel close to the walls was calculated from the continuum energy including the effects of thermal vibrations as given by Eq. (A9) of the Appendix and is also shown in Fig. 1; it is in good agreement with the spacing between successive maxima. As the beam moves into the crystal, the oscillations are damped because the large amplitude trajectories do not all have precisely the same wavelength even in the continuum approximation and also because the discrete nature of the channel walls introduces irregularities in successive half-wavelengths for any one trajectory. Similar calculations for 60-MeV iodine ions in gold show the same type of oscillations with almost the same half-wavelength but with much stronger damping. The stronger damping for iodine in gold arises from the greater range of wavelengths for trajectories near the walls which in turn is due to the shorter screening length in that case.

The depth dependence near the surface for a beam of 10-MeV protons incident along [011] in tungsten is shown in Fig. 2. The behavior is similar to that in Fig. 1 but less regular. The irregularity as compared with the planar case stems from the irregular way in which a trajectory moves from row to row in two dimensions rather than from plane to plane in one. As in the planar case the maxima

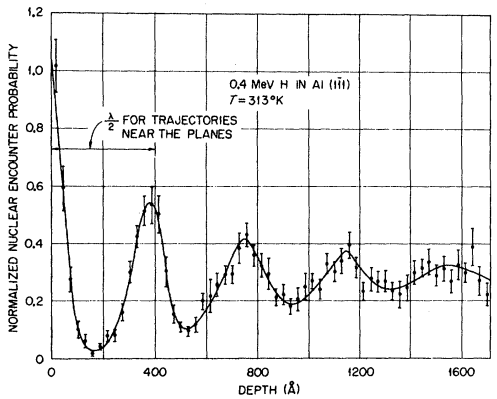

FIG. 1. Nuclear encounter probability as a function of distance from the crystal surface for a beam of particles incident in a planar direction.

and minima are produced by the trajectories that strike the surface near the rows and produce the peak at zero depth. The continuum potential energy at the rows after averaging over thermal vibrations was calculated from Eq. (A7) to be 600 eV. When these trajectories move away from the rows and this amount of potential energy is converted to kinetic energy, the trajectories will make an angle of 0.44° with the row direction. From this angle and the geometry of the crystal, it can be estimated that the trajectories must move somewhat more than 370 Å into the crystal before encountering the nearest-neighbor rows.[21] This corresponds well with the first peak below the surface. The second peak is located a similar distance further into the crystal and can be associated with the second-nearest-neighbor rows. The greater height of the second peak can be attributed to the greater number of second-nearest-neighbor rows and to the additional possibility of trajectories going from the original row to the second-nearest-neighbor rows or back to the original row by bouncing off the first-neighbor rows. Subsequent peaks are presumably due to higher-order groups of rows.

Wavelengths and maximum angles of trajectories to channeling directions could be obtained from measurements similar to the calculations shown in Figs. 1 and 2 and would be quantities of interest. Most measurements, however, lack sufficient depth resolution to give as much detail as shown in those figures. To convert measurements to actual wavelengths or angles, the energy loss experienced by the trajectories producing the maxima and minima, which one would expect to be higher than the random energy loss, is needed rather than the random loss. In addition to the intrinsic interest in these oscillations, an awareness of them is advisable when measuring or calculating minimum yields so that the oscillations can be avoided or averaged over in some suitable way.

B. Bulk Region

Deep in the bulk of the crystal the depth dependence of the nuclear encounter probability for both axial and planar channeling takes the form of a relaxation towards the random value. This relaxation is found experimentally[7] to be approximately an exponential function of depth, characterized by half-thicknesses for the most open directions of a few micrometers for planar channeling and a few tens of micrometers for axial channeling. Calculations with the present program for planar channeling give an exponential relaxation with depth, but the half-thickness is several times larger than observed experimentally. This discrepancy may be due in part to the absence of defects in the model lattice, but is more likely due to the absence from the calculations of scattering of the ions by electrons. Feldman,[22]

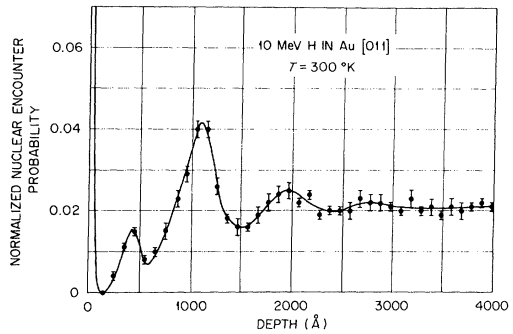

FIG. 2. Nuclear encounter probability as a function of distance from the crystal surface for a beam of particles incident in an axial direction.

Schiøtt,[23] and Van Vliet[24] have shown that electrons rather than nuclei dominate the multiple scattering for ions whose trajectories have small to medium amplitudes of oscillation in the channels. Only for trajectories with large amplitudes is nuclear scattering dominant. The present calculations, which include nuclear multiple scattering only, allow most trajectories to stay channeled too deeply into the crystal.

Other discrepancies between the Monte Carlo calculations and experimental results also suggest the importance of the electronic multiple scattering. When a well-collimated beam of 10- to 60-MeV iodine ions is incident on a thin gold crystal in a planar channeling direction, the emergent beam is elongated perpendicular to the plane of the channel. On comparison with the angular spread of the observed spot, the spread computed by the Monte Carlo program is found to be too small by a factor of 2.[25] After 1- to 10-MeV protons pass through a thick silicon crystal in a planar channeling direction, the beam emerges elongated parallel to the plane. The mean-squared angular spread for 5-MeV protons in the (022) channel of silicon is observed to be 1.7×10^{-3} deg$^2/\mu$m,[26] whereas the Monte Carlo calculations only give a value of 1.4×10^{-4} deg$^2/\mu$m. These two comparisons reinforce the depth-dependence results concerning the need to incorporate electronic multiple scattering into the program.

C. Shoulders of Dips

Another aspect of the depth dependence, the variation with depth of the shoulders of channeling dips, is shown in Fig. 3. For orientations corresponding to the shoulder region, all trajectories are able to penetrate into the rows of atoms, and the multiple scattering will be dominated by the nuclei. The results of Fig. 3 compare favorably with the experimental results of Andersen and Uggerhøj.[27] It should be noted that their experiments were done for [001] rather than [111] but that the target, pro-

jectile, and energy were the same as for Fig. 3. The apparent leveling off of the calculation deep in the crystal at 1.2 rather than 1.0 is due to the influence of nearby planar channels. Results at larger angles show that there is a gradual approach to 1.0.

IV. CRITICAL ANGLES

The term critical angle has been used in the past with several related but different meanings. For clarity it seems best in the present paper to avoid a term with such multiple connotations and to give a separate name to each concept. The first usage of critical angle was by Lindhard[8] to refer to the maximum angle at which a trajectory could be incident on a row or plane of atoms and be deflected by a collective process in a series of collisions with many atoms, giving the effect of deflection by a continuum potential energy. This will be referred to here as the specular angle ψ_s.

The quantity most often measured experimentally is the angle away from a channeling direction at which the nuclear encounter probability is midway between the minimum value along the channeling direction and the value in a random direction. This will be referred to as the half-angle $\psi_{1/2}$. There is no indication that this angle has a fundamental meaning like the half-width of a Breit-Wigner resonance, but it does have a clear definition and can be measured with considerable precision.

Another concept that occurs rather naturally is the breakthrough angle ψ_b, that angle of incidence of an ion on a row or plane that just enables it to surmount the energy barrier and emerge on the opposite side. It has been noted that this angle should correspond to the peak of the shoulder for a planar channel[28,29] but has no apparent correlation with any measurable quantity in the axial case.[29]

A. Previous Results

For axial channeling Lindhard calculated two expressions for the specular angle depending on the energy of the ions. His results were that ψ_s would be

$$\psi_1 = (2Z_1Z_2e^2/dE)^{1/2} \tag{6}$$

for

$$\psi_1 \lesssim a/d \quad \text{or} \quad E \gtrsim E' = 2Z_1Z_2e^2d/a^2 \tag{7}$$

and

$$\psi_2 = 1.5^{1/4}(a\psi_1/d)^{1/2} \tag{8}$$

for $E < E'$. If one looks at the way in which he obtained (6) and (8), it can be seen that (6) applies for conditions in which the screening is relatively unimportant and the interaction is essentially Coulomb in nature. Equation (8), on the other hand, applies for conditions under which the exact nature of the screening is important and is a determining factor in the form of (8). Since the majority of experiments have been performed in the high-energy range, most of the calculations to be reported here have been done in that range, and ψ_2 will be of little interest.[30] In the high-energy range, Lindhard suggested that

$$\psi_{1/2} = C\psi_1 , \tag{9}$$

where C is a constant in the range 1–2. Experiments[7] have shown that Eqs. (6) and (9) give rather accurately the dependence of $\psi_{1/2}$ on Z_1, Z_2, d, and E. The best value of C has generally been found to be about 1.

Equations (6) and (9) give a result for $\psi_{1/2}$ that is independent of temperature. Andersen[10] has extended Lindhard's treatment to incorporate temperature dependence, expressing his results as a series of curves for a wide range of conditions. More recently, Andersen and Feldman[31] have given a formula which expresses this temperature dependence for more restricted conditions. They have also compared Andersen's results with some Monte Carlo calculations for a single row of atoms and found that the two calculations agree quite well. Calculations on the temperature dependence of ψ_s have been performed by Morgan and Van Vliet[32,33] with a Monte Carlo program similar to the present one.

Andersen and Uggerhøj[27] have measured the temperature dependence of $\psi_{1/2}$ for 0.4-MeV protons in tungsten and found agreement with Andersen's calculations. Extensive measurements of $\psi_{1/2}$ for materials with the diamond structure have been made by Picraux *et al.*[9]; they found that the use of Andersen's results on temperature dependence improves the internal agreement among these materials. However, the best value of C to fit their results was 0.75 rather than 1.0 as for a number of other materials, particularly tungsten.

For planar channeling, Lindhard suggested a specular angle of

$$\psi_s = 0.93\psi_a , \tag{10}$$

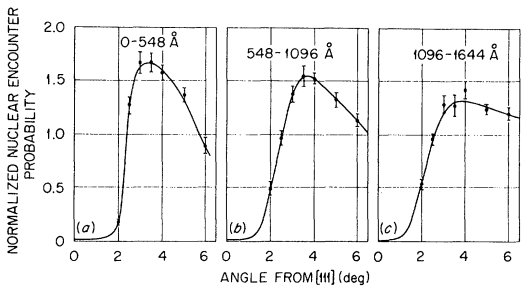

FIG. 3. Depth dependence of the shoulder alongside the dip in nuclear encounter probability for 0.4-MeV protons near [111] in tungsten. The tilt plane was 12° from $(11\bar{2})$ and the temperature was 298 °K.

where

$$\psi_a = (2\pi Z_1 Z_2 e^2 a N d_p / E)^{1/2} \quad (11)$$

and d_p is the spacing between planes. Picraux *et al.*[9] have suggested

$$\psi_{1/2} = 0.60\psi_a , \quad (12)$$

and Picraux and Andersen[11] have incorporated the effect of Lindhard's surface-transmission factor into (12). Experimental planar half-angles have generally satisfied relations such as (10) or (12) reasonably well. The recent measurements of Picraux *et al.* on diamond-lattice materials, however, have shown that (12) satisfactorily describes the dependence on Z_1, Z_2, and E but not on d_p. Picraux and Andersen's calculations give results in accord with the experimentally observed dependence on d_p for these materials.

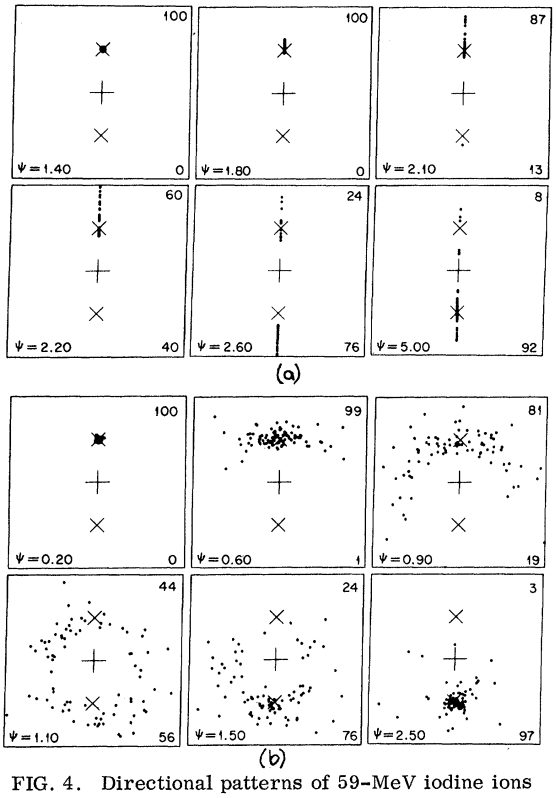

FIG. 4. Directional patterns of 59-MeV iodine ions after encounter with a single [011] row of gold atoms. Each pattern shows the emergent directions for 100 trajectories incident on the row in the plane of the row with the angle ψ shown in the corner of each square. The + symbol indicates the row direction, the lower × marks the incident direction, and the upper × marks the specular reflection direction. The number in the upper right-hand corner is the number of trajectories with emergent directions above the row direction, and the number in the lower right-hand corner is the number with emergent directions below the row. The patterns in (a) are for a static row and those in (b) for a vibrating row with $T = 300\,^\circ$K.

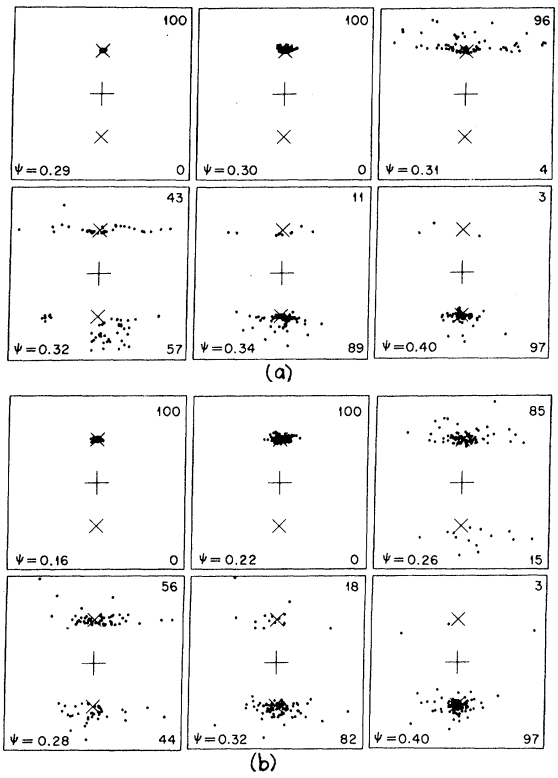

FIG. 5. Directional patterns of 1.4-MeV protons after encounter with a single $(1\bar{1}1)$ plane of aluminum atoms. The remarks in the caption for Fig. 4 apply here also except that trajectories are encountering planes rather than rows, ψ is the angle of inclination of the incident direction to the plane, the direction of incidence is 4.53° from [011], and the temperature for (b) is 313 °K.

B. Breakthrough and Specular Angles

Simple calculations with the present program for the encounters of relatively small numbers of trajectories with single rows or planes of atoms give considerable insight into breakthrough angles and, to a lesser extent, specular angles. Figures 4 and 5 show the results of such calculations for static and vibrating rows and planes. Choices of targets, projectiles, and energies were made as a result of previous calculations,[29,34] but the results are quite general in nature.

For the static row, Lindhard's ψ_1 would be expected to be the specular angle; its value of 1.5° appears to be in good agreement with the Monte Carlo results in Fig. 4(a). If it is assumed that the effect of screening roughly balances the deflections by distant collisions, the shadow angle due to Coulomb scattering for one lattice nucleus should give a value for the breakthrough angle. The shadow angle is $\sqrt{2}\psi_1$,[8] or 2.2° in the present case; again the agreement is good. For the vibrating row

there is no prediction of what the specular angle might be, and Fig. 4(b) indicates that any definition of it would be rather arbitrary. From Eq. (A7) of the Appendix, the breakthrough angle for the vibrating row may be estimated to be 1.16°, a value in good agreement with the Monte Carlo results. It is of interest to note that trajectories incident on the row at an angle near ψ_b tend to emerge randomly around the surface of a cone making the incident angle with the row direction. Trajectories incident at angles much larger than ψ_b penetrate the row readily with multiple scattering much like that for a random orientation.

For planes there is less difference in the results for the static and vibrating cases than for rows. The reflections for $\psi < \psi_b$ are somewhat more specular for the static than the vibrating plane, but the difference is much less marked than it was for the rows. Also, it can be seen that thermal vibrations make considerably less difference in ψ_b. Trajectories incident on the plane at an angle near ψ_b tend to emerge with angles near $\pm\psi_b$ with respect to the plane. The breakthrough angles may be estimated to be 0.314° from Eq. (A2) for the static plane and 0.274° from Eq. (A9) for the vibrating plane; these values agree quite well with the results in Fig. 5.

The comparisons made above serve to illustrate the close correlation noted elsewhere[35] between the breakthrough angle as determined from the analysis of individual trajectories and the breakthrough angle as calculated from the barrier height given by the continuum energy of a row or plane. Also, both Figs. 4 and 5 show that the average energy transverse to the row or plane of atoms is noticeably greater after a close encounter than before it. This increase is due to strong collisions with lattice atoms.

C. Half-Angles

Estimation of half-angles requires much more extensive calculations with the present program, calculations that constitute computer simulations of experiments. Before undertaking such calculations, consideration was given to a number of factors that could influence the results. Measurements of the dip in nuclear encounter probability near an axial direction are made by tilting the beam away from that direction in some "random" plane containing it. Measurements of Andersen and Uggerhøj[27] and previous Monte Carlo calculations[29,34] have shown the variation in the nature of an axial dip with the choice of the tilting plane. Andersen and Uggerhøj's results indicate that there is a variation of half-angle with tilt plane of at least 5–10%. Most experimenters have not specified the orientations of their tilt planes. Two other factors that would be expected to influence the half-angle would be the orientation spread of the beam and the mosaic spread of the crystal. Previous calculations[34] of the $(1\bar{1}1)$ planar dip for 60-MeV iodine in gold have shown that the presence of a mosaic spread causes a slight decrease in the half-angle. The slope of the yield curve near $\psi_{1/2}$ does not produce a variation of $\psi_{1/2}$ with mosaic spread, but the positive curvature does produce a variation. Additional calculations for the [011] axial dip corresponding to the same experimental conditions show that the mosaic spread of 0.13° half-width causes $\psi_{1/2}$ to be $0.82 \pm 0.02°$ rather than $0.77 \pm 0.01°$ as it would have been with zero spread. Figure 6 of Ref. 34 helps to understand this result. The orientation spread in the tilt plane influences $\psi_{1/2}$ just as for the planar dip. However, the spread transverse to the tilt plane tends to increase $\psi_{1/2}$ due to the downward curvature of the yield in the transverse direction. The effect of the transverse spread is dominant because of the stronger curvature in that direction. In measuring a planar dip, a precaution that must be taken is to avoid higher-order axial directions that lie in the plane. Figure 6 illustrates how numerous these are; it is very similar to experimental results of Davies *et al.*[7]

With the above considerations in mind, the following set of conditions was selected for an extensive series of calculations of axial and planar half-angles: (a) beam divergence and mosaic spread of zero; (b) protons incident on tungsten because of numerous experiments on this combination; (c) $E = 10$ MeV to be well into Lindhard's high-energy range; (d) a depth range of 0–5500 Å to average over surface oscillations; (e) a tilt plane 12° from $(11\bar{2})$ for the [111] axial dip, or a tilt plane 8.75° from [111] for the $(01\bar{1})$ planar dip; and (f) temperatures of 4.2, 298, 700, 1200, and 1800 °K.

1. *Temperature Dependence*

Figure 7 shows some calculated temperature effects. The curve through the points for axial channeling was obtained by letting

$$\psi_{1/2} = k[V_{rs}(mu_1)/E]^{1/2} \tag{13}$$

and adjusting k and m to obtain the best fit. V_{rs} is the average potential energy for a static row and is given by Eq. (A1) of the Appendix. It would perhaps be more appropriate to use the vibrating row potential energy V_{rv} rather than V_{rs}. However, the two functions do not differ greatly in the range of interest, so the simpler of the two was chosen. Other authors have previously used either k or m as adjustable parameters, but never both together. It was necessary to adjust both to obtain an adequate fit to the Monte Carlo results; the best-fit values were $k = 0.83$ and $m = 1.2$. Morgan and Van Vliet[33] have found it convenient to express their results on specular angles in terms of a critical approach distance which turned out to be a linear function of the

thermal vibration amplitude. Critical approach distances were found for the present Monte Carlo results, but neither a linear nor a quadratic expression gave a satisfactory relationship to the vibration amplitude. The most satisfactory expression found with which to express the present Monte Carlo results is (13). For future use it will be convenient to have it in the form

$$\psi_{1/2} = kR(mu_1/a)\psi_1 , \tag{14}$$

where

$$R(\xi) = [f_{rs}(\xi)]^{1/2} . \tag{15}$$

Although Eq. (14) indicates that $\psi_{1/2}$ would be infinite for $u_1 = 0$, comparisons with experiment that will be made below show that the values of u_1 in actual solids – including tungsten, which has unusually small thermal vibrations – are sufficiently far removed from this singularity that it causes no problem. However, Eq. (14) may not be used to obtain results for a rigid lattice.

An expression similar to Eq. (14) but with a different function of thermal vibration amplitude in place of the product kR has been given by Andersen and Feldman.[31] If their method is applied to the interaction energy used here, the form obtained for $\psi_{1/2}$ is Eq. (14) with $k = 1.00$ and $m = 1.18$. These values of k and m in (14) give results that lie very close to their formula, with their formula varying somewhat more rapidly with vibration amplitude. However, the values given by each of these formulas are about 25% larger than the Monte Carlo results. In view of the agreement found by Andersen and Feldman between their formula and Monte Carlo calculations for an isolated row, it appears that there is an inherent difference in behavior between a single row and a complete lattice.

In a similar way the curve for planar channeling was obtained by letting

$$\psi_{1/2} = k\{[V_{ps}(mu_1) + V_{ps}(d_p - mu_1) - 2V_{ps}(\tfrac{1}{2}d_p)]/E\}^{1/2} , \tag{16}$$

where V_{ps} is the average potential energy of a static plane, and is given by (A2) of the Appendix. The three terms inside the brackets in (16) represent the energy of the plane on the near side of the channel, the energy of the plane on the far side, and the energy at the center of the channel due to both planes. The second and third terms, particularly the third, are not negligible with respect to the first. Additional such terms exist in Eq. (13) also, but they are small enough to be neglected. The best fit of Eq. (16) to the Monte Carlo results for the planar case was obtained with $k = 0.76$ and $m = 1.6$. It will be convenient to have (16) in the form

$$\psi_{1/2} = kP(mu_1/a,\ d_p/a)\psi_a , \tag{17}$$

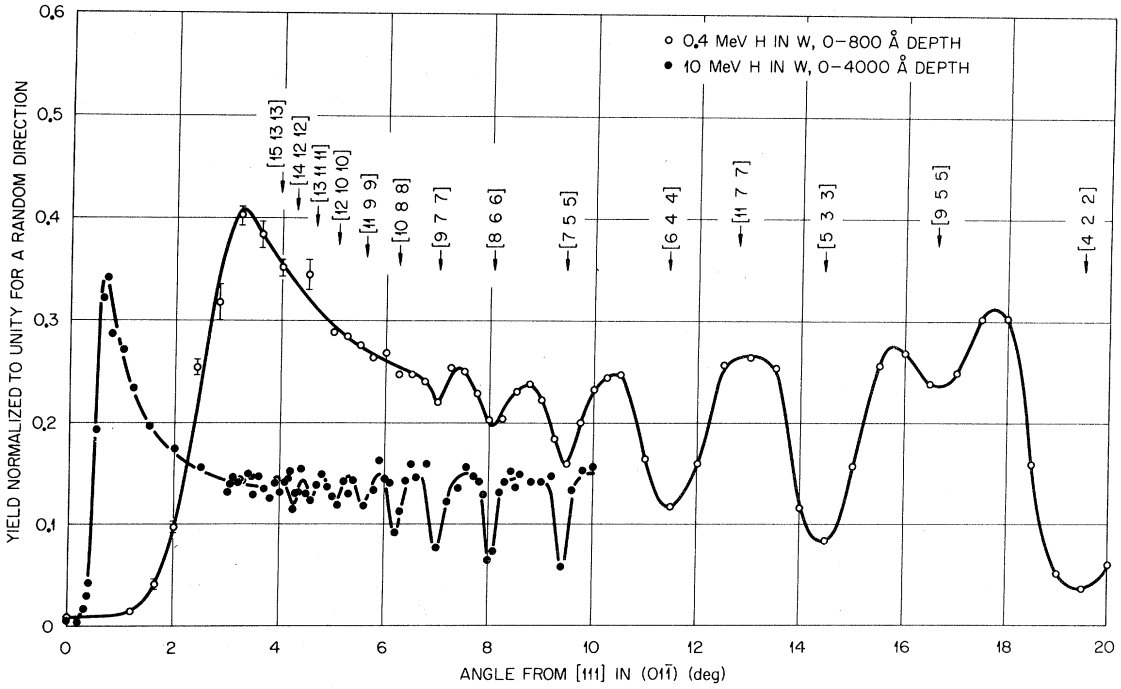

FIG. 6. Nuclear encounter probability as a function of direction in a planar channel. The calculations were done for $T = 298$ °K. Error bars have been omitted on all but a few representative points. Positions of high-order axial directions are marked by arrows. The all even Miller indices, such as [422], are used in place of the smaller equivalent ones, such as [211], so that the row spacings for all directions are given by $\frac{1}{2}d(h^2+k^2+l^2)^{1/2}$.

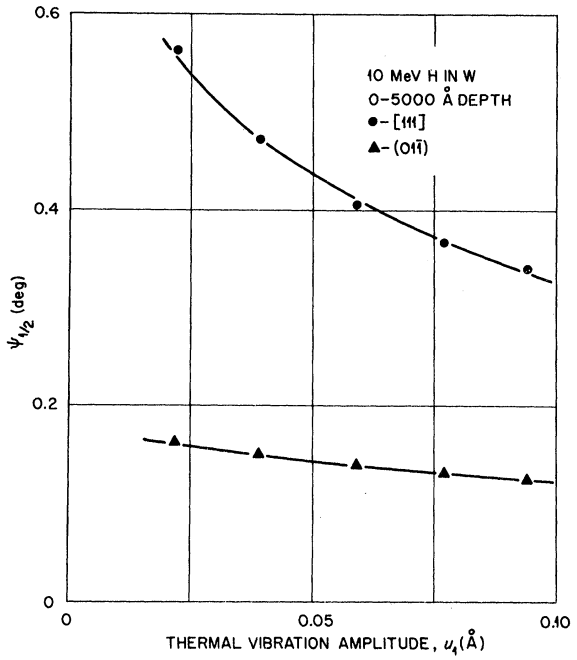

FIG. 7. Half-angles as a function of thermal vibration amplitude for axial and planar channeling. The points are the results of Monte Carlo calculations and the curves are obtained from Eqs. (14) and (17) as explained in the text.

where

$$P(\xi, \eta) = [f_{ps}(\xi) + f_{ps}(\eta - \xi) - 2f_{ps}(\tfrac{1}{2}\eta)]^{1/2} . \quad (18)$$

Although physical intuition suggested Eqs. (13) and (16) as plausible forms for $\psi_{1/2}$, it should be recognized that they have been used to provide empirical curves expressing the results of the Monte Carlo calculations. Caution should be exercised in drawing conclusions therefrom. Also, it should be noted that k and m have been adjusted to fit the Monte Carlo calculations rather than experimental results; agreement with experiment hinges on the adequacy of the interaction energy and other features incorporated in the computer program.

Since R is a function of a single variable it can be conveniently tabulated and is given in Table I. Because P is a function of two variables, it is more conveniently presented as a family of curves; these are shown in Fig. 8.

2. *Energy Dependence*

In addition to the results just given for the temperature dependence, calculations were done to study the dependence on other quantities, principally Z_1 and E. They were done for protons in tungsten for each of several energies and for two choices of crystal thickness. Under the first choice, the thickness was always $2000d$ or about 5500 Å. The second choice was made in such a way that the trajectories would encounter the same number of rows or planes within the crystal thickness at each energy. Accordingly, the thickness was kept at a constant number (between 6 and 7) of half-wavelengths such as shown in Fig. 1. The results are shown in Fig. 9 along with some experimental results of Davies *et al.*[7] The variations of $\psi_{1/2}$ with depth at the various energies are the first such calculated results. The depth dependence of $\psi_{1/2}$ should be much more accurately portrayed than the depth dependence of the nuclear encounter probability along a channeling direction, since the multiple scattering for all trajectories near the half-angle is dominated by the nuclei rather than by the electrons. The transition between Lindhard's high- and low-energy regions occurs at $(Z_1/E)^{1/2} \approx 1.2$ and most of the variation shown is within the high-energy region. In both the axial and planar cases with the thickness set at a constant number of wavelengths, $\psi_{1/2}$ varies within the accuracy of the calculations as $E^{-0.47}$ over the energy range shown. For the constant-thickness calculations, however, no simple power law adequately expresses the energy dependence. Comparison of the calculated and experimental results in Fig. 9 reveals that the two are very close together in the axial case and that the experimental values are slightly but noticeably lower in the planar case. The discrepancy in the planar case may be due in part to the difference in depth at which the Monte Carlo results were calculated and at which the experimental values were measured.

It appears that the difference between $E^{-0.5}$ and

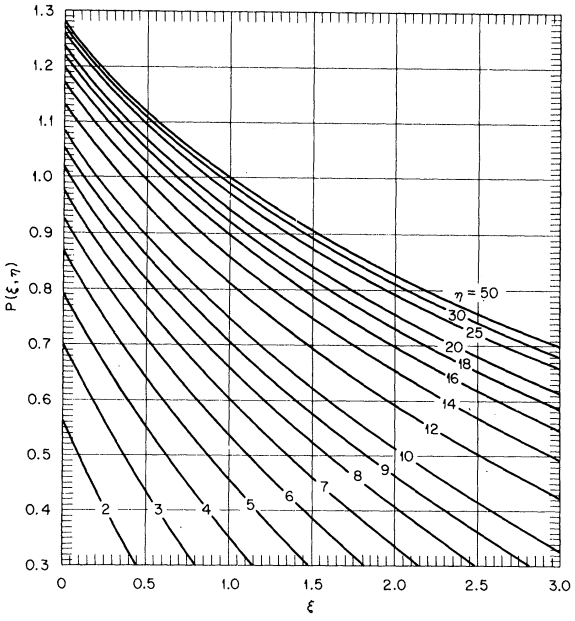

FIG. 8. $P(\xi, \eta)$, defined in Eq. (18), as a function of ξ for various values of η.

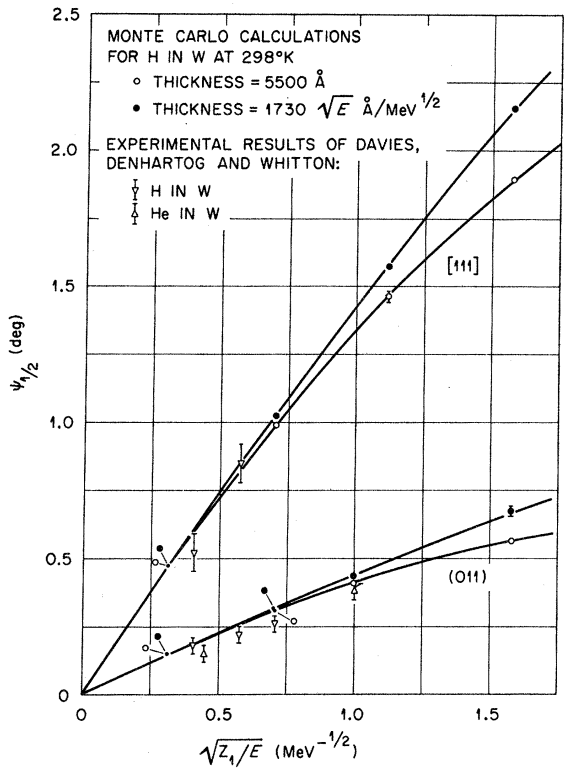

FIG. 9. Dependence of axial and planar half-angles in tungsten on charge and energy of the incident ions.

$E^{-0.47}$ variations of $\psi_{1/2}$ in Fig. 9 is small compared with the experimental uncertainties. Therefore, a straight-line fit in the figure for the calculations over the energy range 1–10 MeV should be an adequate basis for comparison with experimental values. The best fits are obtained by adjusting k in Eq. (14) for the axial case to be 0.80 and k in Eq. (17) for the planar case to be 0.72.

3. *Comparison with Experiment*

Equation (14) has the same dependence on Z_1, Z_2, d, and E as Eq. (9), dependences that have been found to give good agreement with experiment. The defects of Eq. (9) are that $\psi_{1/2}$ is independent of temperature and that C has been found by Picraux *et al.* to depend on the target material. The most relevant experimental measurements of temperature dependence to which Eq. (14) might be compared are those of Andersen and Uggerhøj,[27] for which Andersen's calculations[10] have already been found to give good predictions. The experimental results are shown in Fig. 10 along with several curves calculated from (14) with various parameters. Curve 1 is obtained using the best-fit parameters for 10 MeV. However, the experimental energies fall just below the lower limit of Lindhard's high-energy range so Monte Carlo calculations were done at 0.4 MeV and new values of k and m determined for the best fit to the calculations. The results are shown as curve 2; it has about the right slope but is low in over-all value. To get some measure of the discrepancy in magnitude, k was arbitrarily adjusted to give the best agreement between the calculated and measured values at both energies; curves 3 and 4 are the results of this adjustment. This increase of k by about 14% is just within the range of variation observed by Andersen and Uggerhøj for various tilt planes. Inasmuch as the experimental results do not show the energy dependence that would be expected, the discrepancy between the Monte Carlo calculations and the measured values is greater for 0.48 than for 0.4 MeV. Equation (14) appears to be in reasonable agreement with the temperature dependence of $\psi_{1/2}$ as measured by Andersen and Uggerhøj since the calculated slope is correct, the calculated values are within the range of experimental uncertainty even though at its limits, and numerous other comparisons to be enumerated below show good agreement with experiment. More recently, Foti *et al.*[36] have reported on measurements with 1-MeV protons of the temperature dependence of $\psi_{1/2}$ near the [011] and [111] axes in silicon. The temperature variation calculated from (14) appears to be somewhat less than they measured. The magnitudes of the calculated half-angles are in good agreement with their results for [111] but considerably lower than theirs for [011]. This difference for the two axes reflects the fact that they did not obtain the inverse-square-root dependence on d usually found[9] for $\psi_{1/2}$. Their observed ratio for half-angles in the two directions was 1.39, whereas 1.11 would be expected.

To evaluate how Eq. (14) with the values of k and m determined above from the temperature and energy dependences for protons in tungsten agrees with experiment, comparisons with measured values[7,9,34,37–39] for a large number of elemental ma-

TABLE I. $R(\xi)$ as defined in Eq. (15).

ξ	0.0	0.1	0.2	0.3	0.4	0.5	0.6	0.7	0.8	0.9
0	∞	1.607	1.388	1.251	1.149	1.068	1.001	0.944	0.894	0.849
1	0.810	0.774	0.742	0.712	0.685	0.659	0.636	0.614	0.594	0.575
2	0.557	0.541	0.525	0.510	0.496	0.483	0.470	0.458	0.446	0.435
3	0.424	0.414	0.404	0.395	0.386	0.377	0.369	0.360	0.353	0.345
4	0.338	0.331	0.324	0.317	0.310	0.304	0.298	0.292	0.286	0.280

terials were made. The measurements were selected to represent a wide variety of ions, targets, and experimenters. For axial channeling, comparisons are shown in Table II with the same k and m used for all lattice types. The calculated values for tungsten tend to be slightly less than the measured ones, particularly for the heavier ions, but the differences are generally within the error limits. For protons in tungsten, the product kR in Eq. (14) has the value 0.90, in fairly good agreement with the value 1.0 that has generally been found to be satisfactory for this ion-target combination. Actually, Eq. (9) gives better agreement with the extensive measurements of Davies *et al.*[7] if 0.9 is used for C rather than 1.0. The agreement between calculated and measured values is good for the other target materials, particularly for the semiconductors, with no systematic deviations apparent.

The Z_1, Z_2, and E dependences of planar half-angles as given by Eq. (17) are the same as those given by (10) or (12) and are in agreement with experiment. The temperature dependence calculated for the planar case is less than for the axial case, and there are no experimental values to compare it with. Equation (17), because of the factor P, has a different dependence on d_p than (10) or (12). The variation with d_p given by Eq. (17) using the values of k and m determined above for protons in tungsten is compared for three planar channels in silicon with the experimental results of Picraux *et al.*[9] in Fig. 11; the agreement is good. Picraux and Andersen[11] have also been able to explain the dependence of $\psi_{1/2}$ on d_p by including Lindhard's transmission factor. The concepts involved in the transmission factor are basically the same as those involved in choosing the three terms in the brackets

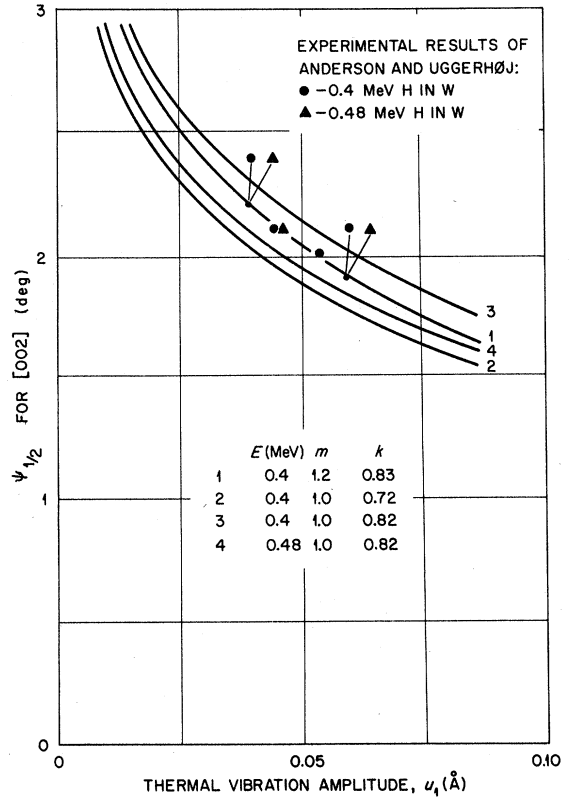

FIG. 10. Temperature dependence of $\psi_{1/2}$ for axial channeling of protons in tungsten. The curves are calculated from Eq. (14) as explained in the text.

TABLE II. Comparison of calculated and measured values of $\psi_{1/2}$ for axial channeling. The calculated values were obtained from Eq. (14) using $k = 0.80$ and $m = 1.2$ and calculating a from Eq. (3a) for $Z_1 = 1, 2$ and from (3b) for $Z_1 > 2$.

Target	Direction	Ion	Energy (MeV)	$\psi_{1/2}$(deg) Calculated	Measured	Ref.
Al	⟨011⟩	H	1.4	0.45	0.42	37
Al	⟨011⟩	H	0.4	0.84	0.90±0.10	38
W	⟨111⟩	He	5.49	0.87	0.85±0.05	39
			6.00	0.83	0.80±0.05	
			7.68	0.74	0.75±0.10	
Au	⟨011⟩	I	60.0	0.80	$1.0 \pm 0.1_5$	34
W	⟨002⟩	H	2.0	0.95	1.00±0.07	7
			3.0	0.78	0.79±0.07	
			6.0	0.55	0.55±0.07	
		He	2.0	1.34	1.39±0.07	
			10.0	0.60	0.67±0.07	
		C	10.0	0.98	1.10±0.07	
			30.0	0.57	0.64±0.07	
		O	10.0	1.13	1.23±0.07	
			30.0	0.65	0.70±0.07	
		Cl	10.0	1.60	1.82±0.07	
			30.0	0.93	1.00±0.07	
	⟨111⟩	H	3.0	0.83	0.85±0.07	
			6.0	0.59	0.52±0.07	
	⟨024⟩	H	3.0	0.52	0.51±0.07	
		He	10.0	0.40	0.42±0.07	
		C	30.0	0.38	0.36±0.07	
		Cl	30.0	0.62	0.70±0.07	
Si	⟨011⟩	H	3.0	0.30	0.26±0.07	7
Au	⟨011⟩	Cl	20.0	0.84	1.10±0.07	7
Si	⟨011⟩	H	0.25	1.03	1.02±0.06	9
			0.5	0.73	0.68±0.06	
			1.0	0.51	0.53±0.06	
			2.0	0.36	0.36±0.06	
		He	0.5	1.03	1.10±0.06	
			1.0	0.73	0.75±0.06	
			2.0	0.51	0.55±0.06	
Ge	⟨011⟩	He	1.0	0.93	0.95±0.06	9
C(dia)	⟨011⟩	H	1.0	0.53	0.54±0.06	9
		He	1.0	0.75	0.75±0.06	

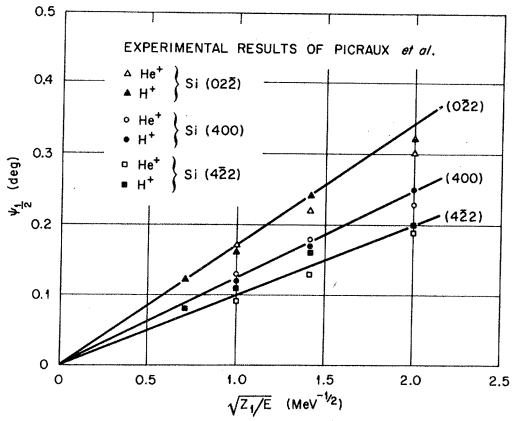

FIG. 11. Variation of half-angle with ion charge and energy for three planar channels in silicon. The estimated error for the experimental points is ±0.03. The Miller indices were chosen so that the interplanar spacings are given by $d/(h^2+k^2+l^2)^{1/2}$ rather than using smaller equivalent ones such as $(0\bar{1}1)$ in place of $(0\bar{2}2)$. The straight lines were obtained from Eq. (17) using $k=0.72$ and $m=1.6$.

in Eq. (16). The present approach, embodied in (16), makes the physics of the problem more apparent and yields a formula by which $\psi_{1/2}$ can be calculated. Also, no arbitrary adjustable parameter such as Picraux and Andersen used for the (011) channel is needed here to get agreement with experiment.

Further comparisons of calculated and measured half-angles for planar channeling are shown in Table III. The agreement in this table and in Fig. 11 is quite good in the case of silicon and germanium. For tungsten, the calculated values tend to be somewhat higher than the measured ones. As noted above in discussing Fig. 9, this discrepancy for tungsten may be due to the depth dependence of $\psi_{1/2}$. Picraux *et al.* extrapolated their values of $\psi_{1/2}$ back to zero depth for silicon and germanium, whereas Davies *et al.* did not do so for tungsten. Furthermore, Picraux *et al.* found the extrapolation to be much more important for the target of higher atomic number. If this represents a definite trend with atomic number, it increases the likelihood that such extrapolation would have given higher values for tungsten. Another possible reason for the discrepancy in the case of tungsten might be an inadequacy of the potential function used. Comparison of Eqs. (14) and (17) indicates that the half-angle formula has a different dependence on the screening length and hence on the screening function in the planar case than in the axial case. An inadequacy of the screening function in calculating half-angles might show up in making comparisons for planar but not for axial half-angles. However, it does not seem justified to seek a resolution of this discrepancy for tungsten by some modification of the screening function. There is a trend in the opposite sense in the case of gold, although the gold measurements are fewer in number and carry less weight.

A tendency was noted above for the calculated values of axial half-angles to be greater than the measured ones in the cases of the heavier ions. The agreement in these cases is improved if a for Eq. (14) is calculated by (3a) for $Z_1>2$ as well as for $Z_1=1$, 2. Appleton *et al.*[40] have found just such a form of the screening length to be in best accord with their measurements of energy losses for various ions in gold. However, consistency here requires the same treatment for planar half-angles, and comparisons such as in Table III for the heavier ions are in general worse if (3a) is used in place of (3b). Considering the axial and planar cases to-

TABLE III. Comparison of calculated and measured values of $\psi_{1/2}$ for planar channeling. The calculated values were obtained from Eq. (17) using $k=0.72$ and $m=1.6$ and calculating a from Eq. (3a) for $Z_1=1$, 2 and from (3b) for $Z_1>2$. The error limits for the measurements are ±0.03 for all cases. Further comparisons are shown in Fig. 11.

Target	Direction	Ion	Energy (MeV)	$\psi_{1/2}$(deg) Calculated	Measured	Ref.
W	⟨002⟩	H	2.0	0.25	0.22	7
			3.0	0.20	0.17	
			6.0	0.14	0.12	
	⟨011⟩	H	2.0	0.32	0.26	
			3.0	0.26	0.22	
			6.0	0.18	0.18	
	⟨002⟩	He	2.0	0.35	0.27	
			10.0	0.16	0.14	
	⟨011⟩	He	2.0	0.45	0.38	
			10.0	0.20	0.15	
	⟨002⟩	C	10.0	0.25	0.20	
			30.0	0.14	0.12	
	⟨011⟩	C	10.0	0.32	0.28	
			30.0	0.18	0.16	
	⟨002⟩	O	10.0	0.29	0.25	
			30.0	0.17	0.15	
	⟨011⟩	O	10.0	0.36	0.33	
			30.0	0.21	0.17	
	⟨002⟩	Cl	10.0	0.40	0.30	
			30.0	0.23	0.22	
	⟨011⟩	Cl	10.0	0.50	0.42	
			30.0	0.29	0.25	
Si	⟨004⟩	H	3.0	0.07	0.07	7
	⟨022⟩	H	3.0	0.10	0.09	
Au	⟨002⟩	Cl	20.0	0.27	0.31	7
	⟨022⟩	Cl	20.0	0.21	0.24	
	⟨111⟩	Cl	20.0	0.30	0.32	
Ge	⟨022⟩	He	0.5	0.44	0.40	9
			1.0	0.31	0.30	
			1.9	0.23	0.23	
	⟨004⟩	He	1.0	0.23	0.18	
	⟨224⟩	He	1.0	0.18	0.20	

gether, Eq. (3b) is to be preferred in the present calculations over (3a) for calculating screening lengths for ions with $Z_1 > 2$.

Tables II and III show that Eqs. (14) and (17) with the choices made for the screening lengths and for the parameters k and m give generally satisfactory predictions of axial and planar half-angles. Picraux *et al.*[9] have suggested that an equation such as (14) can be generalized to a diatomic lattice or to a row having nonuniform spacing by using average values of Z_2 and d. They make a number of comparisons to confirm this idea. The use here of an average potential energy as a basis for Eq. (14) is quite in accord with their suggestion. For planar half-angles, the use of an average value of Z_2 in Eq. (17), as also suggested by them, should likewise be a valid generalization. However, it is not clear that use of the average planar spacing is valid.

V. MINIMUM YIELD

When an ion beam is exactly aligned with a set of rows or planes in a target crystal, the normalized nuclear encounter probability has a minimum value generally called the minimum yield χ.

A. Row Minimum Yield

For an axial direction, Lindhard[8] predicted that the minimum yield just below the surface would be

$$\chi = Nd\pi u_2^2 + Nd\pi a^2 + \chi_3 , \tag{19}$$

where

$$u_2 = \langle x^2 + y^2 \rangle^{1/2} = 2^{1/2} u_1$$

and χ_3 is a contribution from the divergence produced in the beam by scattering in any amorphous region on the surface of the specimen. Most experimental results have been much larger than the values predicted by the first two terms on the right-hand side of Eq. (19), which is not surprising since surface layers were likely present and no particular care was taken to ensure the proper depth resolution. The minimum yields measured by Bøgh[41] and by Appleton and Feldman[42] in tungsten are probably the best published values since tungsten is relatively free of impurity layers on the surface and they made careful measurements of the depth dependence. Their measured values are in satisfactory agreement with the first two terms on the right-hand side of Eq. (19).

1. *Temperature Dependence*

A series of calculations was done with the present program for 3-MeV protons in tungsten at several temperatures and beam divergences to see whether there would be agreement with Eq. (19). In order to avoid the surface peak, the minimum yield was computed for the depth range 340–1370 Å. A Gaussian distribution of beam directions was used as an approximation to experimental situations; its spread is specified by its variance Δ. The calculated values are plotted in Fig. 12. A straight line provides a good fit for each beam divergence, particularly the smaller ones. However, there are two deviations from Eq. (19). The first is that the contribution from beam divergence is primarily to the slope rather than to the intercept of each line in Fig. 12. The second deviation is that the constant term is much smaller, in fact, practically zero,[43] relative to the linear term than predicted by (19). The results of the calculations can be expressed rather well by the form

$$\chi = Nd\pi [C(\Delta) u_2^2 + C'(\Delta) a^2] . \tag{20}$$

From Fig. 12 it can be seen that $C' \lesssim 0.1C$, so that to a good approximation

$$\chi = C(\Delta) Nd\pi u_2^2 . \tag{21}$$

A least-squares fit to the calculations for $\Delta = 0°$ yields the values $C(0) = 3.0 \pm 0.2$ and $C'(0) = 0.2 \pm 0.1$. Calculations for several other ion-target combinations yield similar results. In general, it seems possible to use $C(0) = 3.0 \pm 0.3$ and $C'(0) \approx 0$.

Some insight into the predominance of the temperature-dependent term and the large value of the coefficient C can be obtained by considering the way in which various factors contribute to χ. The first

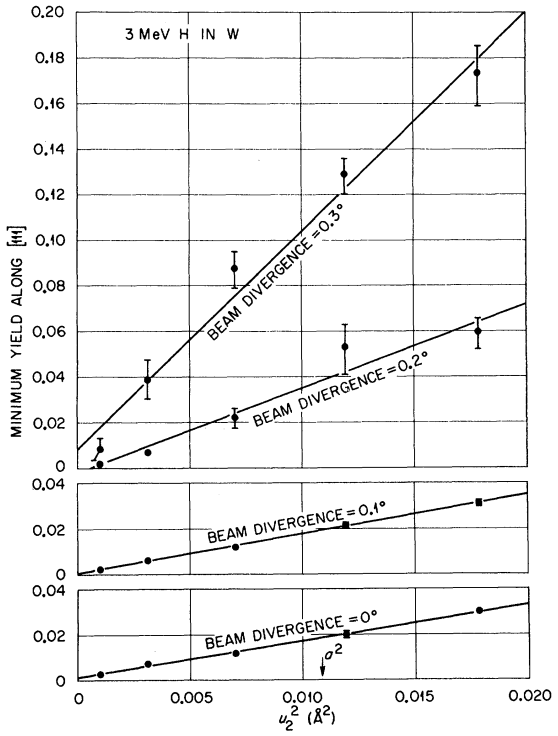

FIG. 12. Minimum yield in an axial direction as a function of thermal vibration amplitude squared for several beam divergences.

to consider is the effectiveness factor $F(E)$, defined as the ratio of the nuclear encounter probability for trajectories having a certain transverse energy E or maximum angle of inclination relative to the rows to the nuclear encounter probability for trajectories having random orientations to the rows. The only method available for calculating this factor is the Monte Carlo program; some results are shown in Fig. 13(a). The effectiveness factor is greater than 1 near and above the maximum value of the continuum potential energy. The other factor to consider is the density of trajectories $D(E)$, defined by letting the fraction of trajectories with energies between E and $E+dE$ be $D(E)dE$. Examples of this quantity are shown in Fig. 13(b). The curve for the discrete-lattice model was calculated by the Monte Carlo program, and the one for the continuum-row model was calculated using Eq. (A8) of the Appendix. For the latter case the energy is that of a vibrating row, $V_{rv}(r)$, and D is given by

$$D(V_{rv}) = \pi u_2^2 N d \left(\frac{dV_{rv}}{d\sigma}\right)^{-1}, \qquad (22)$$

where $\sigma = r^2/u_2^2$. The derivative on the right-hand side of Eq. (22) is a function of u_2; however, calculations at several temperatures show the dependence to be very weak over a considerable range down from the maximum energy. Therefore, the dependence of D, and hence of χ, on u_2 is very nearly quadratic, in accord with the results shown in Fig. 12. Figure 13(c) shows the product of the effectiveness factor times the density of trajectories for each model. The area under the curve in each case gives the minimum yield. The value for the continuum-row model is about two-thirds that for the discrete-lattice model. The difference arises from the trajectories that have been shifted upward in energy – and hence to a higher effectiveness factor – by strong collisions in the Monte Carlo calculations. The simple geometrical model shown in Fig. 13(c) results from assuming an effectiveness factor of 1 for all trajectories that strike within u_2 of the row and an effectiveness factor of 0 for all others. This model gives the same result as Lindhard's treatment of thermal vibrations, namely, the first term on the right-hand side of Eq. (19). From Fig. (13) three reasons can be seen for the large value of C. First, trajectories with transverse energies near and somewhat above the maximum of the continuum potential energy are more effective in making close nuclear encounters than are random trajectories. Second, trajectories with energies considerably below the maximum make a significant contribution by virtue of being very numerous. Third, strong collisions shift trajectories to higher transverse energies and larger effectiveness factors. This last contribution, which is essentially the one considered by Lindhard[8] as leading to the second term on the right-hand side of Eq. (19), also varies quadratically with u_2, presumably due to the form of $D(E)$, rather than being independent of u_2 as obtained by him. The influence of beam divergence on the minimum yield can be seen by considering its influence on the density of trajectories. Beam divergence has the effect of replacing either of the curves in Fig. 13(b) by one that at any energy is some appropriate weighted average of the one shown from that energy downward. For a Gaussian distribution of beam directions, the average is taken over an energy range $\sim E\Delta^2$. If, as in Fig. 12, $E\Delta^2$ is sufficiently small, the resulting increase of the density of trajectories at a given energy is approximately proportional to u_2^2, since the original density has such a proportionality. Therefore, the main influence of beam divergence in Fig. 12 is on the slopes of the lines. On the other hand, as will be discussed below, the divergence produced by a surface layer is much broader and produces a different behavior.

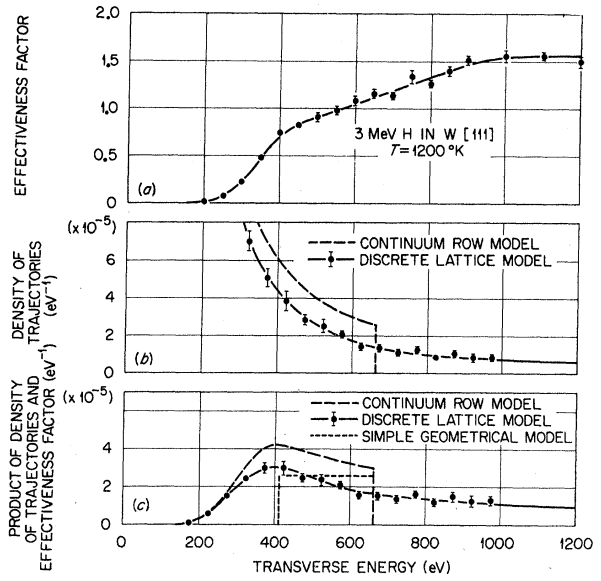

FIG. 13. Factors contributing to the minimum yield for axial channeling.

2. *Energy Dependence*

When Lindhard originally wrote down Eq. (19), he stated that it would only be valid for conditions satisfying Eq. (7). He suggested a low-energy form for the second term in (19); it has an inverse-square-root dependence on energy but differs in other respects from the form given below in (26). In order to test the conditions under which Eq. (21) is valid, a series of calculations was done for protons of various energies in tungsten. The results are shown in Fig. 14(c) along with the previously discussed results at various temperatures in 14(d).

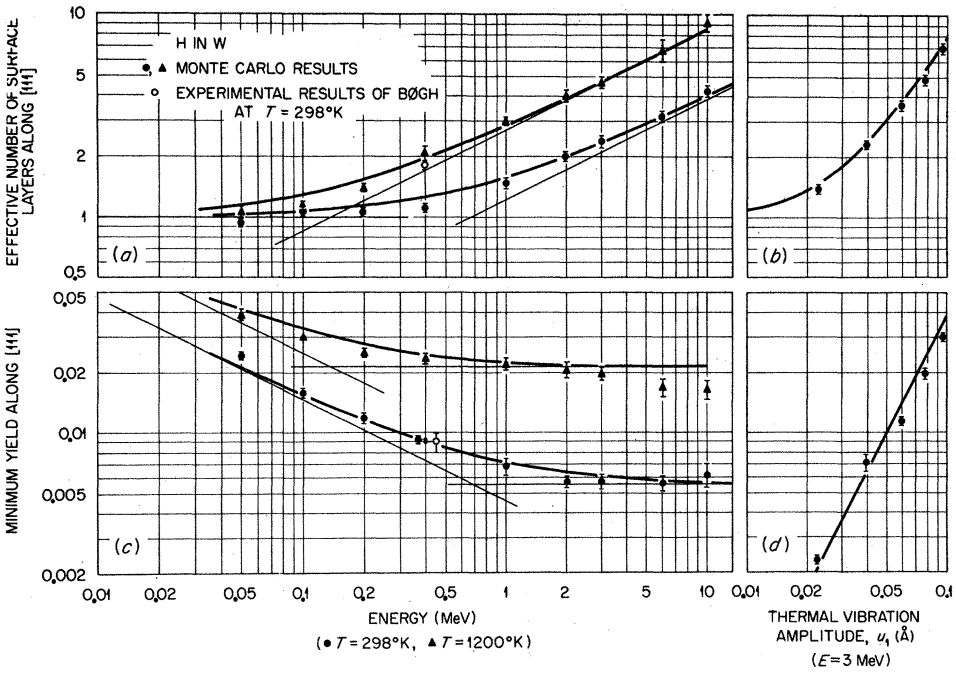

FIG. 14. Dependence of minimum yield and effective number of surface layers in axial channeling on energy and thermal vibration amplitude.

Also shown, in 14(a) and 14(b), is the effective number of surface layers L, which is defined to be the area under the surface peak in a plot such as Fig. 2 divided by the row spacing d. Since L is easier to understand, consider it before χ. At low energies it will have the value 1. At higher energies it might be expected to be of the form $L = \zeta$, where

$$\zeta = \kappa u_1 / (\psi_{1/2} d) \tag{23}$$

and κ is a proportionality constant to be determined empirically. The simplest function found to provide a good connection between the low- and high-energy ranges is

$$L = (1 + \zeta^2)^{1/2} . \tag{24}$$

The intersection of the two asymptotes for $T = 298\ ^\circ\mathrm{K}$ at $E = 0.7$ MeV was used to evaluate κ as 2.2. The curves in Figs. 14(a) and 14(b) were evaluated from Eqs. (23) and (24) with this value of κ. It is interesting to note that the high-temperature asymptotic form of the curve in 14(b) is approximately $L \propto u_1^{1.2}$. The exponent 1.2 rather than 1 is due to the temperature dependence of $\psi_{1/2}$.

It might be expected that L and χ would be related by

$$\chi \propto L \psi_{1/2} \propto L/\zeta . \tag{25}$$

From Eq. (21) the constant of proportionality can be determined so that (21) can be generalized to

$$\chi = C(\Delta) N d \pi u_2^2 (1 + \zeta^{-2})^{1/2} . \tag{26}$$

This relation was used to calculate the curves in Figs. 14(c) and 14(d). For the curves in Figs. 14(a) and 14(c) with $T = 298\ ^\circ\mathrm{K}$, there might be some question as to whether the high-energy region corresponds to $\zeta > 1$ or to Eq. (7) since κu_1 has nearly the same value as a. However, for the curves with $T = 1200\ ^\circ\mathrm{K}$ these two conditions are fulfilled for different energies and it can be seen that $\zeta = 1$ divides the two energy ranges.

For very low energy combined with very low vibration amplitude, Eq. (26) fails to express the Monte Carlo results. This is shown by the lowest-energy point on the lower-temperature curve in Fig. 14(c) as well as by results not plotted. This failure may be due to the $C'(\Delta)$ term in Eq. (20), which has been neglected in the later equations. On the higher-temperature curve in Fig. 14(c) the two highest-energy points may also indicate that (26) is not adequate to express the Monte Carlo results for high energy combined with large vibration amplitude. No reason for this to be true is apparent. Although the exact limits of validity for (26) have not been found, it appears to cover a very wide range of experimental conditions.

3. *Comparison with Experiment*

As mentioned above, the most accurate published experimental results for minimum yields appear to be Bøgh's[41] value of $(0.9 \pm 0.1)\%$ for 0.4-MeV protons directed along [111] in tungsten and Appleton and Feldmans'[42] value of 1.0% for 1-MeV helium ions along [011] in tungsten; Lindhard's formula is in satisfactory agreement with these measurements. As can be seen from Fig. 14(c), the Monte Carlo calculations and Eq. (26) also agree quite well with

Bøgh's result and the energy dependence makes a significant contribution to the calculated result. When allowances are made for differences of projectile, energy, and atomic spacing along the row, Appleton and Feldman's value is in excellent agreement with Bøgh's result and the present calculations The agreement between the present calculation and Lindhard's formula for the conditions under which χ has been measured in tungsten is a consequence of the small value of u_2 relative to a and to the energy of the projectile in this particular case. In general, Eq. (26) will give a value larger than will Lindhard's expression. Although this will be in the right direction to make (26) nearer to agreement with measurements on other materials, it should be kept in mind that these materials almost certainly have sizable contributions from amorphous surface layers.

The agreement between theory and experiment is not so good, however, as the comparisons just made seem to indicate. The value of 400 °K used for the Debye temperature was selected from a convenient source before it was appreciated how sensitive the minimum yield is to the thermal vibration amplitude. Another, perhaps more authoritative, source[17] suggests a value of about 320 °K. When this Debye temperature is used, the theoretical result is approximately 30% higher for the experimental conditions of Bøgh and of Appleton and Feldman. Also, in both experiments the measured effective number of surface layers is higher than calculated by theory, implying the presence of amorphous oxide or impurity layers on the crystal surface. From this result it would seem that the minimum yield for an absolutely clean surface would be somewhat lower than measured by Bøgh or by Appleton and Feldman. A very likely reason for the resulting discrepancy between theory and experiment is that no account has been taken of what difference there may be between the rates of energy loss for the particles contributing to the minimum yield and for particles directed at random in the crystal. Allowance for a higher loss rate for the minimum-yield particles than for the random particles would bring the theoretical and experimental values closer together.

In thinking about channeling, it is often convenient to picture the ion beam inside the crystal as composed of channeled and unchanneled fractions with the channeled fraction getting no nearer to the rows or planes of the lattice than some minimum-impact parameter $r_{\min}$. The results given above in Eqs. (14), (17), and (26) each suggest a minimum impact parameter for a row or plane, as distinguished from an individual atom, that is proportional to u_2. The proportionality constant would be different in each case, ranging from 0.8 to 1.7. Morgan and Van Vliet[33] have expressed some of their results in terms of $r_{\min}$ and found that the relation between $r_{\min}$ and u_2 might be either linear or quadratic depending on the property of interest. Two recent experiments[44] have given estimates regarding minimum-impact parameters. Davies *et al.* have interpreted their results on x-ray yields of channeled ions as evidence that Lindhard's suggestion of $r_{\min} \approx a$ is correct; however, their experiments would not be able to distinguish between the form suggested by Lindhard and forms such as suggested by the present calculations or those of Morgan and Van Vliet. Altman, Feldman, and Gibson have inferred from their experiments on energy losses of 5-MeV protons traversing Si (022) channels that $r_{\min} \approx \frac{1}{2} a \approx u_1$ and say that this result suggests the thermal vibration amplitude may constitute a critical distance parameter for channeling. The present calculations together with the other results on $r_{\min}$ make it appear that critical approach distances for channeling defined in various ways by various means of observation will differ somewhat from each other, and that any expression which may be generally applicable can only be approximate – perhaps only an order-of-magnitude estimate.

4. *Contribution of Surface Region*

In view of the above results, measurements of the energy dependence of the minimum yield are very desirable. Because it is virtually impossible to have a crystal with no amorphous surface region, allowance must be made for its contribution to the energy dependence. An estimate can easily be made if the amorphous region is treated as a random solid. Significant scattering requires close impact so that the potential of the bare nuclear may be used. If it is assumed that scattering through an angle of $\psi_{1/2}$ or greater is required for a contribution to the minimum yield, the resulting estimate of the contribution of the amorphous region to the minimum yield is[8]

$$\chi_3 = \sum_s n_s N d\pi [Z_1 Z_s e^2/(E\psi_{1/2})]^2 , \qquad (27)$$

where the index s runs over the types of atoms in the surface region and Z_s is the atomic number and n_s the number of layers of type s. In Eq. (27), χ_3 has a weak dependence on temperature through $\psi_{1/2}$ and an inverse first-power dependence on E. These dependences are in contrast to the results in Figs. 12 and 13 and stem from the much broader beam spread in the present case. The contribution of the amorphous surface layer to L is

$$L_3 = \sum_s n_s (Z_s/Z_2)^2 . \qquad (28)$$

Monte Carlo calculations of the effect of an amorphous surface region were done also. Equations (27) and (28) agree quite well with them. By making simultaneous measurements of χ and L over a range of energies it should be possible to determine the

contributions to each from the amorphous surface layers and from the underlying lattice itself.

5. *Double Alignment*

When an experiment is conducted so that the incident beam is subject to channeling by being aligned with an axial direction and the emergent beam is subject to blocking by also having the detector aligned with an axial direction, the number of particles scattered into the detector is even further reduced from the number scattered if merely one alignment is made.[42,45-47] When only the beam or detector direction is aligned with a crystal axis, the technique is referred to as single alignment; when both are aligned, the technique is referred to as double alignment. Either may be used to measure amounts of impurities or defects in a crystal; however, the double-alignment technique is more sensitive by one or two orders of magnitude. Feldman and Appleton[42,47] have shown that a modification of Lindhard's theory of the single-alignment minimum yield χ leads to the expression

$$\chi' = (2 - \tfrac{1}{2}\sin^2\alpha)\chi^2 \tag{29}$$

for the double-alignment minimum yield χ', where α is the angle between the detector and beam directions.

The present program has been used to calculate values of χ'. For reasons that will become apparent shortly, such a calculation tends to require a large amount of computer time. Therefore, the following steps were taken to keep this need as small as possible: (i) Statistical uncertainties up to 10% were accepted. (ii) Since the effect can be calculated with better accuracy for larger thermal displacements, gold was selected as the target material. The beam direction selected was [011], the most open direction for this lattice. (iii) The depth necessary to avoid surface effects varies as the square root of the energy, but the yield will be energy dependent at very low energy. Hence, an energy of 1 MeV was chosen as being about the lowest value at which the yield would be independent of energy. (iv) The scattering events used to calculate the yield were those that occurred between 150 and 635 Å. This range avoids the surface peak and first minimum and satisfactorily averages over the deeper maxima and minima. (v) The dependence on thermal vibration amplitude was studied by using only two temperatures, 298 and 1200 °K.

The calculation of χ' was done in two steps. The first found the probability that an incident ion would strike a lattice atom, and the second computed the probability that a scattered ion would reach the detector. For this approach one would write

$$\chi' = \chi_a\chi_b, \tag{30}$$

where χ_a and χ_b are the probabilities for the two steps. It can be seen that χ_a is just the single-alignment minimum yield χ. The computation of χ_b is the more time-consuming part of the problem. While calculating a very accurate value of χ_a, a record was made of the thermal displacement of each struck lattice atom. A lattice atom was considered to be struck if the impact parameter was less than one-quarter of a screening length. Previous calculations[34] have shown the cross section for such an event to be geometrical. After recording a large number of such events, a second series of calculations was done in which trajectories were started within a few degrees of the detector direction. The detector was assumed to have an acceptance angle of about $0.3\psi_{1/2}$, and a record was kept of the fraction of trajectories reaching it. This fraction was χ_b. As a compromise between accuracy and computing time, the starting directions for the second series of calculations were kept within about $3\psi_{1/2}$ of the detector direction and the contribution from trajectories starting at larger angles from the detector was estimated from the Rutherford scattering law. This estimated correction was only ~5% of the total value. Calculations were done for beam-detector angles of 90° and 180°.

The method just described for determining χ_b is a blocking calculation using the special distribution of starting points selected during the calculation of χ_a. Since this is a very inefficient method of calculating χ_b, an alternative method was also tried. This method started with an analysis of the displacements of the struck-atom positions recorded during the χ_a calculation. As would be expected, the distribution parallel to the incident direction was Gaussian with a variance equal to u_1. Within the statistical error limits imposed by the finite sample size, the distribution in each of the two directions perpendicular to the incident direction also appeared to be Gaussian but had a variance equal to $1.16u_1$. With the distribution of struck atoms known, a channeling calculation could be done, and χ_b could be equated to the results by means of the reversibility rule.[8,27,48] In the channeling calculation, u_1 in Eq. (5) was replaced by $1.16u_1$, but the distribution given by Eq. (1) was not altered. The second method of calculating χ_b is much faster than the first, but uncertainties in the distribution of struck atoms leave them with about the same accuracy. The two methods agree quite well.

The results of the double-alignment calculations are summed up in the relation

$$\chi' = \nu(\alpha)\chi^2, \tag{31}$$

where $\nu(90°) = 1.1 \pm 0.1$ and $\nu(180°) = 1.2 \pm 0.1$. The magnitude of $\nu(\alpha)$ is smaller and its variation with α is less in (31) than in Feldman and Appleton's formula given in (29). Bøgh[49] has measured a value of $\chi' = 4\times10^{-4}$ for 1-MeV helium ions in tungsten us-

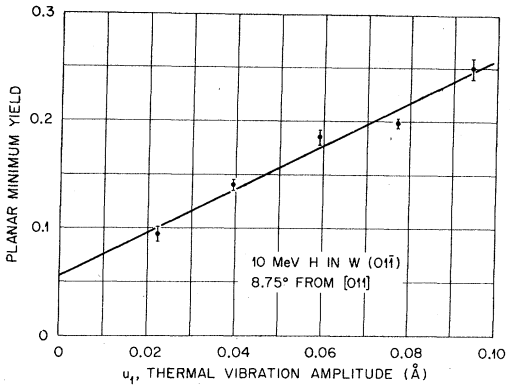

FIG. 15. Minimum yield in a planar direction as a function of thermal vibration amplitude.

ing ⟨111⟩ axes. Also for 1-MeV helium in tungsten, Appleton and Feldman have measured a value of 9×10^{-4} at room temperature as well as values at several other temperatures using ⟨001⟩ axes[42] and a value of 4×10^{-4} using ⟨111⟩ axes.[50] Equation (31) predicts a value of 1×10^{-4} for ⟨111⟩ axes and 1.3×10^{-4} for ⟨001⟩ axes. The measured and calculated values show a large difference in magnitudes and fairly good agreement in rates of temperature variation.[42] Part of the difference in magnitude may be accounted for by very thin oxide or impurity layers that the experimenters believe to be present, but it is unlikely that this can account for the entire difference. Also, as discussed above for single-alignment minimum yields, a more accurate value of the Debye temperature may decrease the difference somewhat, while inclusion in the calculation of energy-loss rates may increase the difference.

B. Planar Minimum Yield

Lindhard[8] has given for the minimum yield in planar channeling the expression

$$\chi = 2a/d_p, \tag{32}$$

which is independent of energy and temperature. The measured values of Davies *et al.*[7] are considerably higher than predicted by (32). A series of calculations was done with the present program to see how the results would agree with the experimental values and to see how the minimum yield might depend on various parameters. The results for the temperature dependence are shown in Fig. 15 along with a linear least-squares fit to the calculations. In contrast to the results for the axial case, the planar minimum yield shows a linear (or even slower than linear) dependence on u_1 and the value of χ at $u_1 = 0$ is not negligible. No analysis in terms of a density of trajectories and an effectiveness factor has been made. Figure 16 shows the energy dependence of the minimum yield and effective number of surface layers along with the temperature dependence of these quantities. Because the values of L due to the perfect lattice are large for planar channeling, amorphous surface layers should make relatively small contributions to χ. From Figs. 16(a) and 16(c) it appears that L and χ satisfy Eq. (25), but no other empirical analytical expressions for them have been found in the planar case. Davies *et al.*[7] observed that the energy dependence of χ for protons in tungsten was negligible over the energy range 2–6 MeV and did not quote the energy at which

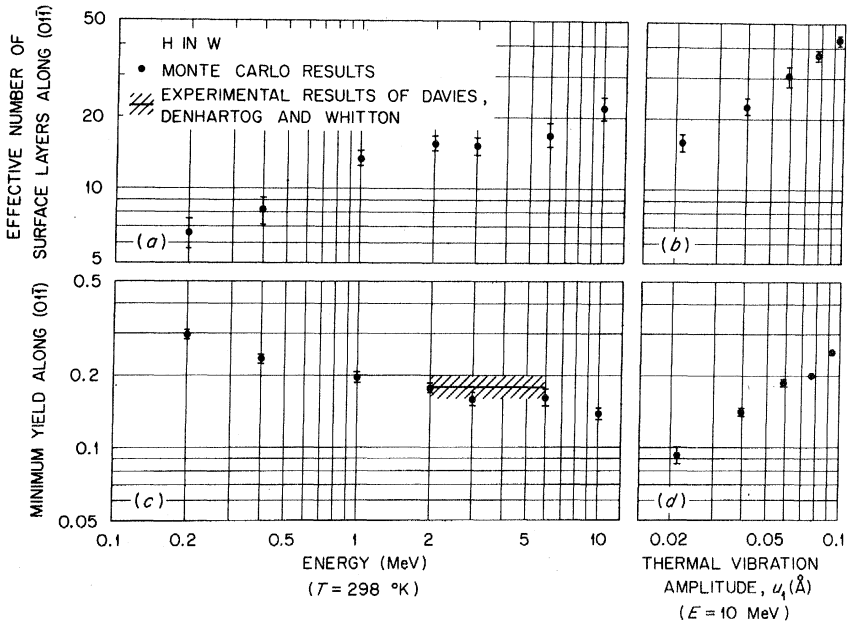

FIG. 16. Dependence of minimum yield and effective number of surface layers in planar channeling on energy and thermal vibration amplitude.

their reported value was measured. Their observation is compatible with the weak calculated energy dependence. The agreement with the experimental values is much better for the present calculations than for Lindhard's formula. The same remarks made above about the influence of the Debye temperature and the rate of energy loss on the predicted value of the minimum yield in axial channeling also apply here for planar channeling.

VI. CONCLUSION

The main results of this paper are given in Eqs. (14) and (17) for axial and planar half-angles and in Eqs. (26) and (31) for axial single- and double-alignment yields. These formulas have been obtained as empirical fits to calculations made with the Monte Carlo computer program described in the paper. Figures 1 and 2 also show important results on variations of yield with depth that occur near the surface of a crystal. Equations (14) and (17) with Table I and Fig. 8 offer a quite accurate and convenient method of calculating half-angles. Difficulties with earlier formulas noted by Picraux *et al.*[9] are resolved by these equations. Whereas the present results for half-angles are similar to but more accurate than earlier ones, the result given in Eq. (26) for the single-alignment minimum yield differs considerably from the previous one due to Lindhard. The present form has an energy dependence as well as a much stronger temperature dependence. A relationship has also been found between the minimum yield and the yield from the surface of the crystal; it is expressed as Eq. (25). Lindhard's expression for the minimum yield gives equally good results for tungsten, for which the most accurate measurements have been made, but Eq. (26) should give better results for other materials having larger thermal vibration amplitudes. Although the form of the double-alignment minimum yield given by (31) does not agree in magnitude with experiment, it is superior, particularly for temperature dependence, to what was previously available.

For the model on which the computer program is based, half-angles can be calculated by the Monte Carlo technique with a precision of better than 1%, and presumably Eqs. (14) and (17) are almost equally precise. Experimental uncertainties are sometimes as low as 5% but are generally 10% or greater. More precise experiments in the future may reveal inadequacies of the model. One possibility is that axial half-angles for different lattice types might not be calculable with one set of values for k and m. This would not be surprising since the portion of an axial dip from around $\psi_{1/2}$ out to beyond the shoulder has been shown[29] to be shaped by the shoulders of the various planes that pass through the axis. It is even possible that different axes in one lattice type would have different k's and m's because of the differing sets of planes. Other reasons the theory might fail to agree with more accurate experiments are inadequacies in the potential-energy function, lack of correlation between the thermal vibrations of the lattice atoms, or some other feature of the model. More accurate measurements to further probe the theory would certainly be desirable. In order that additional experiments provide the best possible test of the theory, the location of the tilt plane and the depth range in the crystal over which the measurements were made should be reported, and the divergence of the beam, mosaic spread of the crystal, and amorphous surface layers should be minimized with the residual values of these latter features measured and characterized as accurately as possible.

It would also be desirable to test the new predictions on energy and temperature dependence of the minimum yield by additional measurements and to have better measurements on materials other than tungsten. Target materials should be selected to be as free as possible from amorphous surface layers, and the measuring technique should have sufficient depth resolution to avoid any influence of surface variations on the minimum yield. In turn the theory needs to have the energy loss incorporated into it and to make use of the best available value of Debye temperature. Electron multiple scattering could be conveniently incorporated along with the energy loss, which should improve the predictions of the theory regarding the dechanneling distance and patterns of emergent beams.

ACKNOWLEDGMENTS

The author is most grateful to M. T. Robinson for many useful suggestions concerning the computer program and to him as well as O. S. Oen, T. S. Noggle, D. K. Holmes, and B. R. Appleton for stimulating discussions of channeling.

APPENDIX: CONTINUUM POTENTIAL ENERGIES

In addition to their direct use to interpret experiments, continuum potential energies in which the discrete charges of the lattice atoms are imagined to be distributed uniformly along a row or plane of atoms are useful in understanding the results of the Monte Carlo calculations presented above and in providing formulas by which such results may be summarized.

For the energy of Eq. (2), Erginsoy[51] has given the continuum energy for a static row as

$$V_{rs}(r) = (2Z_1Z_2e^2/d)\, f_{rs}(r/a) \qquad \text{(A1)}$$

and the continuum energy for a static plane as

$$V_{ps}(r) = (2\pi Z_1Z_2e^2a/A)\, f_{ps}(r/a), \qquad \text{(A2)}$$

where

$$f_{rs}(u) = \textstyle\sum_i \alpha_i K_0(\beta_i u) \ , \qquad \text{(A3)}$$

$$f_{ps}(u) = \sum_i \gamma_i e^{-\beta_i u} \quad , \tag{A4}$$

A is the area per atom in the plane, K_0 is a modified Bessel function, $\gamma_i = \alpha_i/\beta_i$, and all other quantities are as defined following Eq. (2) or before Eq. (5).

For a vibrating row, the continuum energy may be obtained by combining Eqs. (1) and (A1), giving

$$V_{rv}(r) = (2Z_1Z_2e^2/d)\, e^{-r^2/2u_1^2} \sum_i \alpha_i\, g_i(r/u_1) \quad , \tag{A5}$$

where

$$g_i(u) = \int_0^\infty K_0(\beta_i \mu u')\, I_0(uu')\, e^{-u'^2/2}\, u'\, du' \quad , \tag{A6}$$

$\mu = u_1/a$, and I_0 is also a modified Bessel function. For the value $u = 0$, the integral in (A6) can be done in closed form with the results[52]

$$g_i(0) = \tfrac{1}{2} e^{\tau_i} E_1(\tau_i)$$

and

$$V_{rv}(0) = (2Z_1Z_2e^2/d) \sum_i \tfrac{1}{2} \alpha_i e^{\tau_i} E_1(\tau_i) \quad , \tag{A7}$$

where $\tau_i = \frac{1}{2}\beta_i^2\mu^2$ and

$$E_1(x) = \int_x^\infty y^{-1} e^{-y}\, dy$$

is the exponential integral.

For nonzero values of u, the integral in Eq. (A6) has been evaluated both by numerical quadrature and by expansion in a power series. The power series is obtained by expanding I_0 in (A6); the result is

$$g_i(u) = \sum_{n=0}^\infty \frac{u^{2n}}{2^n n!^2}\, \mathcal{J}_n(\tau_i) \quad ,$$

where

$$\mathcal{J}_n(\tau_i) = \int_0^\infty K_0(2\tau_i^{1/2} t^{1/2}) t^n e^{-t}\, dt \quad .$$

The first two $\mathcal{J}$'s are

$$\mathcal{J}_0 = \tfrac{1}{2} e^{\tau_i} E_1(\tau_i) \quad ,$$

$$\mathcal{J}_1 = \tfrac{1}{2}[(1+\tau_i) e^{\tau_i} E_1(\tau_i) - 1] \quad ,$$

and the higher $\mathcal{J}$'s can be found from the recursion relation,

$$\mathcal{J}_{n+1} = (2n + 1 + \tau_i)\, \mathcal{J}_n - n^2 \mathcal{J}_{n-1} \quad ,$$

which is valid for $n \geq 1$. The power-series result is

$$V_{rv}(r) = \frac{2Z_1Z_2e^2}{d}\, e^{-\sigma} \sum_{n=0}^\infty C_n \sigma^n \quad , \tag{A8}$$

where $\sigma = \frac{1}{2}r^2/u_1^2$ and

$$C_n = \sum_i \alpha_i \mathcal{J}_n(\tau_i)/n!^2 \quad .$$

For a vibrating plane, the continuum energy has been obtained by Erginsoy[52] and is

$$V_{pv}(r) = \frac{2\pi Z_1 Z_2 e^2 a}{A} \sum_i \tfrac{1}{2}\gamma_i e^{\tau_i} \times \left\{ e^{-\beta_i r/a}\, \mathrm{erfc}\left[2^{-1/2}\left(\frac{\beta_i u_1}{a} - \frac{r}{u_1}\right)\right] + e^{\beta_i r/a}\, \mathrm{erfc}\left[2^{-1/2}\left(\frac{\beta_i u_1}{a} + \frac{r}{u_1}\right)\right]\right\} , \tag{A9}$$

where

$$\mathrm{erfc}(x) = 2\pi^{-1/2} \int_x^\infty e^{-t^2}\, dt$$

is the complementary error function.

---

*Research sponsored by the U. S. Atomic Energy Commission under contract with Union Carbide Corp.

[1]S. Datz, C. Erginsoy, G. Leibfried, and H. O. Lutz, Ann. Rev. Nucl. Sci. 17, 129 (1967).

[2]M. W. Thompson, Contemp. Phys. 9, 375 (1968).

[3]R. S. Nelson, *The Observation of Atomic Collisions in Crystalline Solids* (North-Holland, Amsterdam, 1968), Chap. 4.

[4]Can. J. Phys. 46, 449–782 (1968).

[5]Brookhaven National Laboratory Report No. BNL-50083 (unpublished).

[6]*Atomic Collision Phenomena in Solids*, edited by D. W. Palmer, M. W. Thompson, and P. D. Townsend (North-Holland, Amsterdam, 1970).

[7]See, for example, J. A. Davies, J. Denhartog, and J. L. Whitton, Phys. Rev. 165, 345 (1968).

[8]J. Lindhard, Phys. Letters 12, 126 (1964); Kgl. Danske Videnskab. Selskab, Mat.-Fys. Medd. 34, No. 14 (1965).

[9]S. T. Picraux, J. A. Davies, L. Eriksson, N. G. E. Johansson, and J. W. Mayer, Phys. Rev. 180, 873 (1969).

[10]J. U. Andersen, Kgl. Danske Videnskab. Selskab, Mat.-Fys. Medd. 36, No. 7 (1967).

[11]S. T. Picraux and J. U. Andersen, Phys. Rev. 186, 267 (1969).

[12]J. Lindhard, Kgl. Danske Videnskab. Selskab, Mat.-Fys. Medd. 34, No. 14 (1965)

[13]See, for example, M. Blackman, in *Encyclopedia of Physics*, edited by S. Flügge (Springer-Verlag, Berlin, 1955), Part I, Vol. 7, p. 377.

[14]A. J. Dekker, *Solid State Physics* (Prentice-Hall, Englewood Cliffs, N. J., 1957), p. 44.

[15]*American Institute of Physics Handbook*, edited by Dwight E. Gray (McGraw-Hill, New York, 1963), p. 4-61.

[16]B. W. Batterman and D. R. Chipman, Phys. Rev. 127, 690 (1962).

[17]*International Tables for X-Ray Crystallography*, edited by Kathleen Lonsdale (Kynoch, Birmingham, England, 1962), Vol. III, p. 234.

[18]G. Molière, Z. Naturforsch. 2a, 133 (1947).

[19]O. B. Firsov, Zh. Eksperim. i Teor. Fiz. 33, 696 (1957) [Soviet Phys. JETP 6, 534 (1958)].

[20]C. Lehmann and G. Leibfried, Z. Physik 172, 465 (1963).

[21]Nearest neighbor will be used here to mean both of the first two rings of neighbors, which are very closely spaced in the face-centered cubic lattice. Likewise second-nearest neighbor will be used to mean the next set of closely spaced rings of neighbors.

[22]L. C. Feldman (private communication).

[23]H. E. Schiøtt (private communication).

[24]D. Van Vliet, AERE Report No. R6395 (unpublished).
[25]T. S. Noggle and J. H. Barrett, Ref. 5, p. 402.
[26]L. C. Feldman, B. R. Appleton, and W. L. Brown, Ref. 5, p. 58.
[27]J. U. Andersen and E. Uggerhøj, Can. J. Phys. 46, 517 (1968).
[28]H. A. Fowler and C. Erginsoy, Phys. Letters 24A, 390 (1967).
[29]J. H. Barrett, Phys. Rev. 166, 219 (1968).
[30]Some recent measurements in Linchard's low-energy range and references to earlier such measurements are reported by I. A. Abroyan, V. A. Koryukin, N. N. Ushakov, and L. A. Tseknovicher, Fiz. Tverd. Tela 11, 3376 (1969) [Soviet Phys. Solid State 11, 2745 (1970)].
[31]J. U. Andersen and L. C. Feldman, Phys. Rev. B 1, 2063 (1970).
[32]D. V. Morgan and D. Van Vliet, Can. J. Phys. 46, 503 (1968).
[33]D. V. Morgan and D. Van Vliet, Ref. 6, p. 476.
[34]T. S. Noggle and J. H. Barrett, Phys. Status Solidi 36, 761 (1969).
[35]Reference 29. The value of ψ_b for the vibrating plane quoted there is slightly smaller than the value given here because a was calculated in the earlier paper from Eq. (3b), whereas (3a) was used for the results given here.
[36]G. Foti, F. Grasso, and E. Rimini, Nuovo Cimento Letters 1, 941 (1969).
[37]J. U. Andersen, J. A. Davies, K. O. Nielsen, and S. L. Andersen, Nucl. Instr. Methods 38, 210 (1965).
[38]E. Bøgh and E. Uggerhøj, Nucl. Instr. Methods 38, 216 (1965).
[39]B. Domeij and K. Bjorkqvist, Phys. Letters 14, 127 (1965).
[40]B. R. Appleton, Sheldon Datz, C. D. Moak, and Mark T. Robinson (unpublished).
[41]E. Bøgh, Phys. Rev. Letters 19, 61 (1967).
[42]B. R. Appleton and L. C. Feldman, Ref. 6, p. 417.
[43]The fact that the straight-line fit passes through the origin within the error limits of the calculation should not be taken to imply that $\chi = 0$ for $u_{\frac{1}{2}}^2 = 0$. The significant portion of the fit is for the physically realizable range of $u_{\frac{1}{2}}^2$: 10^{-3} Å^2 and above.
[44]J. A. Davies, L. Eriksson, N. G. E. Johansson, and I. V. Mitchell, Phys. Rev. 181, 548 (1969); M. R. Altman, L. C. Feldman, and W. M. Gibson, Phys. Rev. Letters 24, 464 (1970).
[45]V. S. Kulikauskas, M. M. Malov, and A. F. Tulinov, Zh. Eksperim. i Teor. Fiz. 53, 487 (1968) [Soviet Phys. JETP 26, 321 (1968)].
[46]E. Bøgh, Can. J. Phys. 46, 653 (1968).
[47]L. C. Feldman and B. R. Appleton, Appl. Phys. Letters 15, 305 (1969).
[48]E. Bøgh and J. L. Whitton, Phys. Rev. Letters 19, 553 (1967).
[49]E. Bøgh, Ref. 5, p. 76.
[50]B. R. Appleton and L. C. Feldman (private communication).
[51]C. Erginsoy, Phys. Rev. Letters 15, 360 (1965).
[52]B. R. Appleton, C. Erginsoy, and W. M. Gibson, Phys. Rev. 161, 330 (1967).

PHYSICAL REVIEW B VOLUME 3, NUMBER 5 1 MARCH 1971

Alpher-Rubin Ultrasonic Attenuation and Dipolar Nuclear-Acoustic-Resonance Coupling in Pure Metals*

J. G. Miller, W. D. Smith,† D. I. Bolef, and R. K. Sundfors
Arthur Holly Compton Laboratory of Physics, Washington University, Saint Louis, Missouri 63130
(Received 27 August 1970)

Experimental results are presented of measurements of the very small magnetic-field-dependent changes in the attenuation $\Delta\alpha$ of ultrasound (absorptive Alpher-Rubin effect) in pure single crystals of Al, Cu, Nb, and Ta. Measurements were made at 293 K in magnetic fields ranging from 0 to 11 kOe, using both longitudinal and transverse acoustic waves. Variations of $\Delta\alpha$ with both orientation and magnitude of the external magnetic field were studied. Measurements of the dependence of $\Delta\alpha$ on frequency over the range 5–250 MHz were made. The results are particularly relevant to the study of induced dipolar coupling in nuclear acoustic resonance. A derivation is given of expressions for the nuclear-acoustic-resonance signal in pure metals.

I. INTRODUCTION

The influence of a magnetic field on the propagation of acoustic waves in solid metals was first considered theoretically by Alpher and Rubin.[1] The Alpher-Rubin phenomenological theory predicts changes in both the acoustic phase velocity (dispersion) and the acoustic attenuation (absorption) when a static magnetic field is applied. Galkin and Koroliuk[2] verified the predicted dependence of acoustic velocity on the magnitude of the magnetic field for longitudinal acoustic waves propagating in polycrystalline tin and aluminum. In a comprehensive study, Alers and Fleury[3] verified the predicted dependence of acoustic velocity on both magnitude and orientation of an external field for longitudinal and transverse 10-MHz acoustic waves. A review of the dispersive Alpher-Rubin effect has been given by Alers.[4]

The magnetic field dependence of the acoustic at-